IEEE Access
Multidisciplinary ⋮ Rapid Review ⋮ Open Access Journal

Received May 15, 2021, accepted May 23, 2021, date of publication June 4, 2021, date of current version June 15, 2021.

Digital Object Identifier 10.1109/ACCESS.2021.3086701

An Approach to Acquire Path-Following Skills by Industrial Robots From Human Demonstration

ANGEL RODRIGUEZ-LIÑAN[1], ISMAEL LOPEZ-JUAREZ[2], ALAN MALDONADO-RAMIREZ[2], ANTONIO ZALAPA-ELIAS[1], LUIS TORRES-TREVIÑO[1], JOSE LUIS NAVARRO-GONZALEZ[3], AND PAMELA CHIÑAS-SANCHEZ[4]

[1]Universidad Autónoma de Nuevo León, Facultad de Ingeniería Mecánica y Eléctrica, San Nicolás de los Garza 66455, Mexico
[2]Centre for Research and Advanced Studies (CINVESTAV), Ramos Arizpe 25900, Mexico
[3]IJ ROBOTICS, Saltillo 25000, Mexico
[4]Tecnologico Nacional de Mexico, Instituto Tecnologico de Saltillo, Saltillo 25280, Mexico

Corresponding author: Ismael Lopez-Juarez (ismael.lopez@cinvestav.edu.mx)

This work was supported in part by the National Council of Science and Technology of Mexico under Grant INFR-2014-01-230761.

ABSTRACT Industrial robots have mainly been programmed by operators using teach pendants in a point-to-point scheme with limited sensing capabilities. New developments in robotics have attracted a lot of attention to robot motor skill learning via human interaction using Learning from Demonstration (LfD) techniques. Robot skill acquisition using LfD techniques is characterised by a high-level stage in charge of learning connected actions and a low-level stage concerned with motor coordination and reproduction of an observed path. In this paper, we present an approach to acquire a path-following skill by a robot in the low-level stage which deals with the correspondence of mapping links and joints from a human operator to a robot so that the robot can actually follow a path. We present the design of an Inertial Measurement Unit (IMU) device that is primarily used as an input to acquire the robot skill. The approach is validated using a motion capture system as ground truth to assess the spatial deviation from the human-taught path to the robot's final trajectory.

INDEX TERMS Learning from demonstration (LfD), inertial measurement unit (IMU), 3D trajectory acquisition.

I. INTRODUCTION

Traditionally, robots have been used in the automotive, electrical, metal, chemical and food industry although some other areas have began using service robots in everyday tasks such as vacuuming, sweeping or grass mowing. Robots are widely used in handling operations, welding, assembly, dispensing (painting, gluing, sealing, spraying, etc.) and processing (such as sand machining for casting). The programming, and reprogramming after positional errors, of such complex operations is very time consuming. Therefore, alternative approaches such as Learning from Demonstration (LfD) have become relevant as they could speed up programming and, eventually, the learning of robot skills. A closer relationship between human operators and industrial robots is envisaged, which would result in an increased need for robots to adapt to their environment, learn from it, and act accordingly. Robots need to not only learn and adapt but also to recover from errors and forget such conditions. In order to embed such knowledge, robots have to perceive their environment through sensors. LfD seeks to enable human users to expand the capabilities of robots through interactive teaching instead of explicit programming.

Generally speaking, LfD deals with two learning stages. The first stage is devoted to high-level learning of a sequence of actions and can be thought of as a planner. At the low-level stage, the robot learns motor skill coordination as pointed out by [1]. Several other approaches to the transferring of motor skills to robots have been reported. Basically, such alternative approaches focus on estimating the orientation and/or position of a desired path. For this, motion capture classification can be established considering the used technology [2].

Several types of sensing devices are not specifically for motion capture, but there are sensors to capture other useful information in aspects related to HRI in programming such as optical information, voice, touch/force, magnetic field, gesture detection, EMG, data gloves, RFID and laser scanners. Those tracking technologies can be grouped in the way

The associate editor coordinating the review of this manuscript and approving it for publication was Heng Wang.

pointed out by Field *et al.* [3]: Optical detection with passive, active markers and markerless systems that rely upon image processing and segmentation to find a human posture matching a fixed human template. Inertial sensors detect linear accelerations and rotational velocities. Other devices, such as exoskeleton-mounted potentiometers, rely on mechanical devices to measure relative joint angles between limbs, then compute motion with kinematics; however, they have trouble detecting the true position and orientation relative to the global frame. Magnetic sensors are based on electromagnetic fields established by transmitting antennae mounted on significant positions on the body giving an estimation of joint positions and angles. Similarly, acoustic sensing works by attaching ultrasonic transmitters and microphones at specific locations on a moving body.

Advantages of IMU-based methods over the optical ones are their flexibility outdoors, fast calibration, portability, and that they do not require structured environments nor sophisticated infrastructure [3]. Some advantages over mechanical sensing (potentiometers) are that it is not constrained by the rigidity of the wearable equipment (as exo-skeletons are) and that it detects events such as jumping or turning. Advantages of IMU devices over magnetic sensing (antennae) are its portability, that metallic objects do not cause noise nor distortion and that they do not require structured environments with RF equipment. Acoustic sensing (as ultrasonic sensors) presents self-occlusion by body parts blocking a direct path to receiving microphones. Frequencies are susceptible to background noise, temperature, humidity and wind (when used outdoors).

A. RELATED WORK

Camera-based systems to detect objects use image processing algorithms, such as the geometric analysis approach (from images) described in [4]–[7]. These cameras could be infrared to detect objects and their depth information. In general, these Computer Vision Systems (CVS) have presented good results in constrained indoor environments; however they are highly sensitive to environmental conditions changes like shadows, occlusions, light intensity variation, reflexes from bright objects, variable distances, etcetera.

Several efforts have been made towards solving the correspondence problem of dealing with the effective mapping of links and joint positions from human to robot. In Table 1, an extended summary of relevant research works and methods are presented in the areas of LfD and computer vision. These works are important since they deal with the problems of learning object-action relations in HRI to combine human and robot capabilities to increase their potential use in improving the flexibility of production lines as pointed by [8].

In Table 1, relevant and specific problems for robot motion using different and specialised sensing systems in LfD are presented, [9]–[18]. The used methods range from Graph Networks to ANN solutions. CVS are widely used as an aid to accomplish the LfD task. Despite the advantages presented with the different sensing devices, IMU-based systems are flexible, portable, insensitive to environmental light changes, acoustic noise, occlusions, and they are not restricted to structured environments using special equipment

TABLE 1. Relevant research works and methods in the area of LfD and computer vision. SOTA = state of the art.

Ref	Problem to solve	Methods	Results
[9]	Learning object action relation from bi-manual manipulation	Graph Networks and RGBD Images	0.86 F1-score classifier for 9 tasks
[10]	Representing robot skills as Motion Primitives	Mixture Density Network	Outperforms SOTA techniques
[11]	Teaching a humanoid robot manipulative tasks	Gaussian Mixture model	Skill Generalisation in different contexts
[12]	To discover and recognise human Motion Primitives	Motion Flux Optimisation	Public data set of human motion primitives
[13]	Humanoid robot control to co-manipulate objects	Dynamic Systems Modeling.	Adaptive behaviours for whole body manipulation
[14]	Accurate robot force tracking	Dynamic Systems Modeling	Perform tasks in uncertain environment where physical interaction is needed
[15]	Humanoid robot for safe collaboration	Engineering	A humanoid robot capable of helping a human in a collaborative task
[16]	Egocentric 3D human pose estimation	Convolutional NNs	SOTA results on predicting human pose from monocular Head Mounted Device
[17]	Communication through a lexicon	Vocabulary of body and hand gestures	bimanual operation using ROS
[18]	Visual search of relevant targets in the environment	Deep Reinforcement Learning	A framework for a robot to complete simple tasks and recover from failures

for detection ([19]–[24]). In IMU-based methods, the position and/or orientation are estimated for two or three axes using accelerometers, gyroscopes and magnetometers. Commonly used methods to compare the accuracy of the IMU data use of special sensors such as the camera-based 3D motion analyzers. IMU devices have widely been used for spatio-temporal gait analysis and their performance compared against motion capture systems [25], [26]. Results have shown that the reliability and accuracy of a low-cost IMU-based system outperformed those obtained from different motion capture systems [27], [28].

In this work, we focus on the low-level stage by proposing the use of an IMU device as input to acquire a motion path guided by human demonstration (for both, position and orientation). The integration of several steps in a single algorithm were included in steps such as sensor calibration, path orientation estimation, motion detection, transformation of the acceleration plot for the sensor to the reference plot and acceleration integration to generate the Cartesian path in order to have an industrial robot imitate a particular motion skill in a simple manner. The development of the algorithm allows its programming in an industrial robot, of which the precision depends on the estimation from the IMU data.

B. ORIGINAL CONTRIBUTION

The human arm does not usually remain in a completely static state, as there are small movements (such as breathing) that must be discarded as a movement event in LfD applications in robots. In this sense, our original contribution is twofold since it uses a novel fusion algorithm based on the variance value for the motion detection to detect static states and also it considers the development of a flexible portable device that is not restricted to structured environments.

The developed algorithm is based on a previously calibrated sensor to capture the human path (position and orientation). The path orientation is obtained after detecting the movement and then transforming the acceleration frame of the sensor into the reference frame. The Cartesian path is corrected using the Zero Velocity Update approximation (ZVU). A transformation is performed from the Cartesian path to the robot workspace and then the joint trajectory is generated using the inverse kinematics of the robot. Finally, the path is programmed and implemented into a real industrial robot. To compare the results, the path generation is evaluated using a motion capture system (*OptiTrack*^{TM}) as a ground truth using different trajectories.

The proposed IMU device represents a low-cost, simple-to-implement alternative for outdoor and indoor applications that overcomes the constraints presented in image-based approaches. Additionally, the IMU does not require special infrastructure, it is portable and can be placed on tools or even over parts of the human body because of their small size and weight (as in exoskeletons), it can detect events such as jumps or twists, and it is cost-effective compared to CVS. The developed device is resistant to varying light conditions, occlusions, and acoustic background noise or wind (when used outdoors).

Our method can be used independently in unstructured environments or to complement other motion caption methods. Considering these conditions, this approach could be more attractive in several other applications, as it has recently been reported in [1], [29]–[32].

This IMU-based platform for motion capture can be embedded in high-level stages of LfD operations where the robot is directed by the human operator to the desired positions by the movements of his body (postures). This high-level stage includes orders such as: Emergency stop with one and two hands, decrease robot speed, increase robot speed, etcetera as reported in [33].

This article is organised as follows: After this Introduction, Section II presents the proposed approach and algorithm estimation of the trajectory using the IMU. In section III, the testbed used during experiments is described as well as the experimental results. Finally, ongoing work and conclusions are provided in section IV.

II. ESTIMATION OF POSITION AND ORIENTATION OF THE HUMAN HAND BY THE IMU DEVICE

In Figure 1, the diagram of the proposed methodology to estimate the position and orientation of the human hand is shown. First, the data from the IMU device held by the operator's hand is processed off-line. After this, the inverse kinematic model of the robot, which is based on its joints' dimensional parameters, is obtained. With these models and the estimation of position and orientation, the inverse kinematics of position and velocity can be obtained, i.e. the joint position and velocity of the robot. Then, a trajectory generation algorithm computes continuous-time functions of the joint variables that are to be programmed into the robot controller. Finally, the resultant path at the low-level of the LfD technique is performed by the robot and recorded to evaluate the performance.

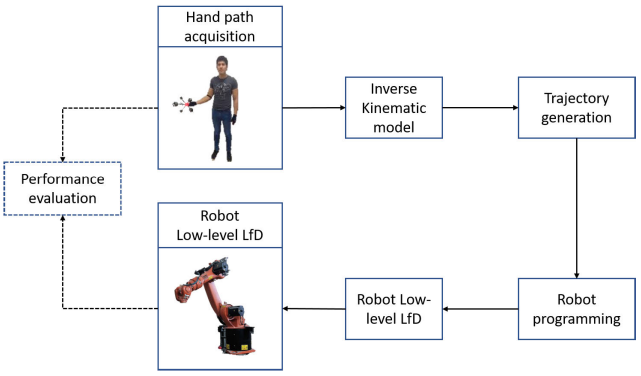

FIGURE 1. Methodology.

The position and orientation of moving objects can be estimated by the IMU devices because they have accelerometers, gyroscopes, and other sensors such as magnetometers and barometers [34]. The position could be calculated knowing

the initial position and computing a double numerical integration of the accelerometer data. However, these measurements have noise and gravity components. Accelerometers and gyroscopes have both advantages and disadvantages. The estimated orientation angles are very accurate if the accelerometer is static, however, if sudden changes occur, the measurements are noisy. On the other hand, the gyroscope is ideal if sudden changes occur in orientation but, if it is in a static position, then the numerical integration methods produce an error accumulation known as drift effect.

The implementation of sensor fusion techniques allows one to take only the advantageous characteristics from each of these sensors to obtain improved angle estimations without noise and accumulative errors. Some examples of these fusion techniques can be found in [19]–[21], [24] for the Kalman Filter (KF) and in [21], [23], [35]–[38] for the Complementary Filter (CF).

In our work, several sensor fusion algorithms for both, the static and dynamic case were studied to select the best option and to implement it in our device. Firstly, an algorithm processes the data from the IMU device to determine whether a movement has occurred. A common approach is to determine whether an object is static simply by noticing whether the acceleration L2-norm value is less than a certain threshold. However, it is difficult for a human being to keep an object in a completely static state since small vibration artifacts (such as breathing) occur. On the other hand, when moving at a constant speed, the acceleration norm is around zero; then, it is difficult to find a threshold value that distinguishes between static state and constant speed comparing only the L2-norm from the acceleration. In this work, a motion detection algorithm is proposed that takes into account the variance value instead of only the L2-norm of the accelerations, giving a better performance when the sensing device is used for trajectories made by human movements. Furthermore, the motion detection is robust under uncertainties due to calibration and force gravity. The proposed approach is depicted in Figure 2, where the use of fusion sensor techniques are considered in order to estimate the position/orientation of the IMU device held by the human operator; it is detailed as follows:

A. DATA READING AND CALIBRATION

The accelerometer data ${}^{I}a_{x,k}$, ${}^{I}a_{y,k}$ and ${}^{I}a_{z,k}$ are measured at sample k in the IMU coordinate frame f_I for the x, y and z axes, respectively. Similarly, angular velocities $\omega_{x,k}$, $\omega_{y,k}$ and $\omega_{z,k}$ are measured from a three-axis gyroscope at sample k about the x, y and z axes of the IMU coordinate frame f_I. Also, the time value t_k is read in sample k.

For the initial calibration, the IMU is required to remain a time window "ini" (few seconds) at rest on a flat surface as perpendicular to the gravity vector as possible. During this stage, the mean of the gyroscope data is computed and it is subtracted to calibrate the gyroscope data around the origin.

Also, the mean of the accelerometer data is computed for each axis during the calibration time, which is labeled as ${}^{I}\bar{a}_{x,ini}$, ${}^{I}\bar{a}_{y,ini}$ and ${}^{I}\bar{a}_{z,ini}$, respectively. After the calibration stage, the IMU orientation is estimated.

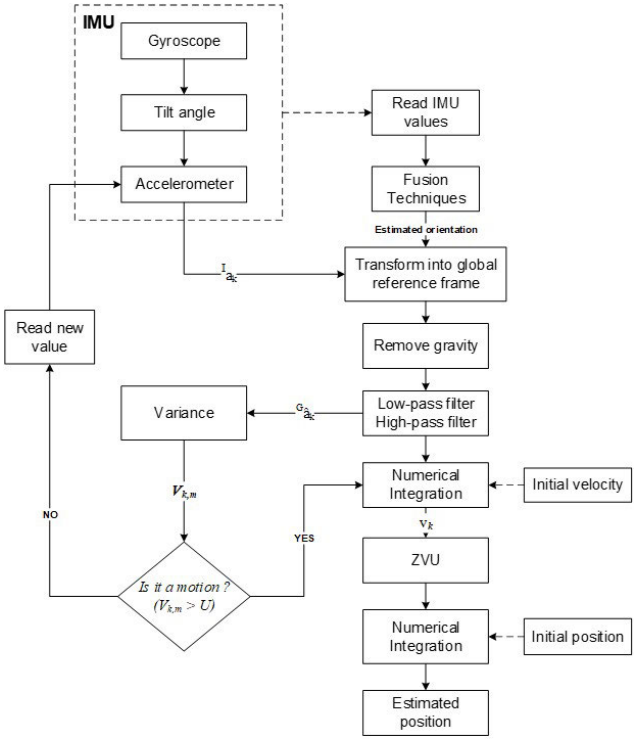

FIGURE 2. Scheme for position estimation.

B. ORIENTATION ESTIMATION

In this work, the sensor fusion uses the data from the accelerometer and the gyroscope to estimate the orientation by means of a Kalman filter.

Based on the accelerations, the estimation is achieved for the Tait-Bryan angles roll ψ_k and pitch ρ_k over x and y axes, respectively, which by means of trigonometry, is

$$\begin{aligned}\psi_k &= atan2\left({}^{I}a_{y,k}, {}^{I}a_{z,k}\right)\\ \rho_k &= atan2\left(-{}^{I}a_{x,k}, \sqrt{{}^{I}a_{y,k}^2 + {}^{I}a_{z,k}^2}\right)\end{aligned} \tag{1}$$

The initial values ψ_{ini} and ρ_{ini} are computed using the initial acceleration mean ${}^{I}\bar{a}_{x,ini}$, ${}^{I}\bar{a}_{y,ini}$ and ${}^{I}\bar{a}_{z,ini}$ in (1). The estimation based only on an accelerometer does not allow one to calculate the angle yaw ϕ_k over axis z, so it will remain at an arbitrarily assigned initial angle yaw ϕ_{ini}.

The gyroscope estimation can be carried out by means of numerical integration of angular velocities, which is represented in the form of a quaternion

$${}^{I}\omega_k = \begin{bmatrix}0 & {}^{I}\omega_{x,k} & {}^{I}\omega_{y,k} & {}^{I}\omega_{z,k}\end{bmatrix} \tag{2}$$

The quaternion derivative describing rate of change of the global frame f_G relative to the sensor frame f_I can be calculated as

$${}^{G}_{I}\dot{q}_{\omega,k} = \frac{1}{2}{}^{G}_{I}\hat{q}_{\omega,k-1} \otimes {}^{I}\omega_k \tag{3}$$

where the operator $\otimes$ denotes a quaternion product, the $\hat{}$ accent denotes a normalised vector of unit length [38]. The orientation of the global frame relative to the IMU frame at sample k can be numerically integrated from (3) as shown in [37], [38]:

$$ {}^{G}_{I}q_{\omega,k} = {}^{G}_{I}\hat{q}_{\omega,k-1} + {}^{G}_{I}\dot{q}_{\omega,k}(t_k - t_{k-1}) \tag{4} $$

The quaternion representation is used to avoid problems associated to the gimbal lock [39]. Then, the normalised orientation quaternion ${}^{G}_{I}\hat{q}_{\omega,k} = [\, q_{w,k}\ q_{x,k}\ q_{y,k}\ q_{z,k}]^T$ is transformed to the rotational matrix ${}^{G}_{I}R$, with

$$ \begin{aligned} {}^{G}_{I}R_{11} &= 1 - 2q^2_{y,k} - 2q^2_{z,k} \\ {}^{G}_{I}R_{12} &= 2(q_{x,k}q_{y,k} - q_{z,k}q_{w,k}) \\ {}^{G}_{I}R_{13} &= 2(q_{x,k}q_{z,k} + q_{y,k}q_{w,k}) \\ {}^{G}_{I}R_{21} &= 2(q_{x,k}q_{y,k} + q_{z,k}q_{w,k}) \\ {}^{G}_{I}R_{22} &= 1 - 2q^2_{x,k} - 2q^2_{z,k} \\ {}^{G}_{I}R_{23} &= 2(q_{y,k}q_{z,k} - q_{x,k}q_{w,k}) \\ {}^{G}_{I}R_{31} &= 2(q_{x,k}q_{z,k} - q_{y,k}q_{w,k}) \\ {}^{G}_{I}R_{32} &= 2(q_{y,k}q_{z,k} + q_{x,k}q_{w,k}) \\ {}^{G}_{I}R_{33} &= 1 - 2q^2_{x,k} - 2q^2_{y,k} \end{aligned} $$

The rotational matrix ${}^{G}_{I}R$ is transformed to the Tait-Bryan angles ϕ_k, ρ_k and ψ_k over z, y and x axes, respectively:

$$ \begin{aligned} \rho_k &= atan2\left(-{}^{G}_{I}R_{31}, \sqrt{{}^{G}_{I}R^2_{11} + {}^{G}_{I}R^2_{21}}\right) \\ \phi_k &= atan2\left({}^{G}_{I}R_{21}/\cos(\rho_k), {}^{G}_{I}R_{11}/\cos(\rho_k)\right) \\ \psi_k &= atan2\left({}^{G}_{I}R_{32}/\cos(\rho_k), {}^{G}_{I}R_{33}/\cos(\rho_k)\right) \end{aligned} \tag{5} $$

If $abs(\rho_k) = \pi/2$, one possible convention is to choose

$$ \begin{aligned} \phi_k &= 0 \\ \psi_k &= sign(\rho_k) \cdot atan2\left({}^{G}_{I}R_{12}, {}^{G}_{I}R_{22}\right) \end{aligned} $$

The orientation estimation is an important stage because it is used to transform information between the sensor coordinate frame f_I and the global coordinate frame f_G. Accelerometer-based estimation is very accurate for static cases, but not for sudden changes. The gyro-based estimation is good for sudden changes, but not for static case. There are different sensor fusion techniques to improve the orientation estimation. A comparison of different methods to estimate the orientation is presented in this paper. After comparing the results, the best method was selected. The orientation impacts the estimation of Cartesian position trajectories when used in the transformation of acceleration data from the sensor frame to the global reference frame. The estimation error of position would increase due to the double integration for position. The following well-known filters were implemented and compared in order to select the best filtering technique:

- Complementary Filter (CF)
- Explicit Complementary Filter (ECF) from [35]
- Descendent Gradient Algorithm (DGA) from [38]

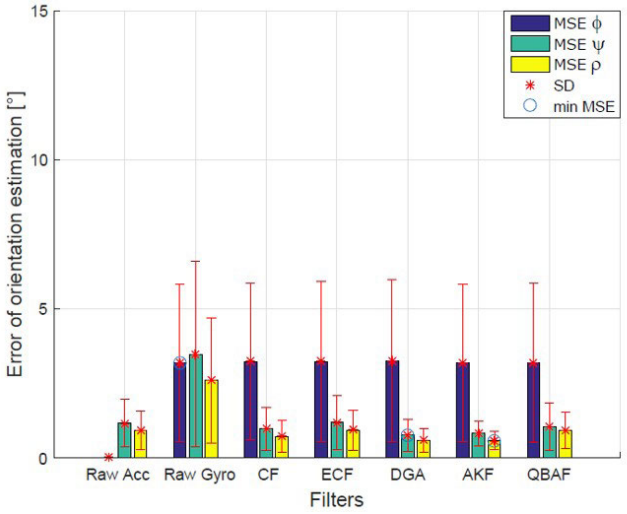

FIGURE 3. Error of orientation estimation for different filters (Static case).

- Adaptive Kalman Filter (AKF) from [40], [41]
- Quaternion-based Adaptive Filter (QBAF) from [37]

Experimental results for orientation estimation using the listed filters were obtained from different tests of rotation and displacement of the proposed IMU device. To illustrate the results on the orientation estimation, quaternions were shown as Tait-Bryan angles ϕ, ρ and ψ over z, y and x axes, respectively. The Mean Squared Error (MSE) and the Standard Deviation (SD) were computed for the comparison between the reference orientation and the estimation with each filter. The MSE and SD are also shown for the raw measurements of the accelerometer (Raw Acc) and gyroscope (Raw Gyro).

These experiments produced different results for the static and dynamic cases of the IMU device. From Figure 3, it can be observed that the results are similar for some filters in the static cases. Some filters fail during motion in the dynamic case as observed in Figure 4. The application of the AKF filter resulted in lower errors in both the static and the dynamic case, so this filter was implemented in the IMU device during tests. The implemented AKF pseudocode algorithm for fusion sensor is given in Appendix A, whereas the filter parameters used during experiments are given in the Appendix B.

C. POSITION ESTIMATION

In order to estimate the Cartesian position, the IMU orientation (ϕ_k, ρ_k, ψ_k) obtained with the AKF is used to transform acceleration vectors ${}^{I}a_k = [\, {}^{I}a_{x,k}\ {}^{I}a_{y,k}\ {}^{I}a_{z,k}]^T$ (for all sample k) from the IMU frame f_I to the global frame f_G, such that

$$ {}^{G}a_k = {}^{G}_{I}R_k\ {}^{I}a_k \tag{6} $$

where ${}^{G}_{I}R_k = Rot_Z(\phi_k)Rot_Y(\rho_k)Rot_X(\psi_k)$ is the rotation matrix at sample k. The gravity compensation subtracts the gravity ${}^{G}g$ on the global reference frame from ${}^{G}a_k$ to derive

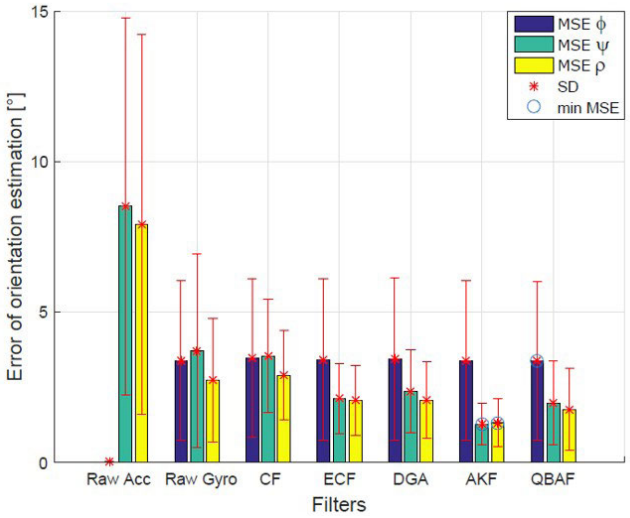

FIGURE 4. Error of orientation estimation for different filters (Dynamic case).

the induced-motion acceleration, that is

$$ {}^{G}a_{m,k} = {}^{G}a_k - {}^{G}g \tag{7}$$

Afterwards, the induced-motion acceleration ${}^{G}a_{m,k}$ is filtered by a low-pass filter in order to eliminate the high frequency noise and a high-pass filter to eliminate residual constant components obtaining the filtered acceleration ${}^{G}\hat{a}_k$.

In this work, the motion detection is proposed by a variance of the filtered acceleration of the IMU data. The variance vector $V_{k,M}$ is computed from ${}^{G}\hat{a}_k$ for each sample k in a time window of M passed samples by

$$ V_{k,M} = \frac{1}{M} \sum_{j=k-M+1}^{k} ({}^{G}\hat{a}_j - {}^{G}\bar{a}_{k,M})^2 \tag{8}$$

where ${}^{G}\bar{a}_{k,M}$ is the mean of the M-samples window ending at sample k, which is given by

$$ {}^{G}\bar{a}_{k,M} = \frac{1}{M} \sum_{j=k-M+1}^{k} {}^{G}\hat{a}_j \tag{9}$$

In case of $k \leq M$, $M = k$ is chosen to compute equations (8) and (9). If $V_{k,M}$ exceeds an appropriately chosen threshold value U, then it is considered that there is a motion, otherwise it is not considered a motion, that is

$$ m_{d,k} = \begin{cases} 1, & \text{if } V_{k,M} > U \\ 0, & \text{if } V_{k,M} \leq U \end{cases} \tag{10}$$

If motion has been detected ($m_{d,k} = 1$), the IMU data is used to estimate the position considering the initial value of the velocity and position. Motion detection could be attempted by comparing the L2-norm or the absolute magnitude of the acceleration with a threshold; however, the use of the variance (8) in (10) resulted to be less sensitive to error changes as it is shown in Section III-B.

Starting from rest, the linear velocity is estimated by numerical integration from the acceleration, taking into account the motion detection. For example, with the Euler method, this velocity vector v_k is computed at time sample k by

$$ v_k = v_{k-1} + (t_k - t_{k-1})\ m_{d,k}\ {}^{G}\hat{a}_{k-1} \tag{11}$$

where g is the gravity acceleration constant. Assuming that there exists R resting points associated to the samples k_l such that $m_{d,k_l} = 0$ with $l = \{1, 2, \ldots, R\}$. The drift velocity $v_{d,k}$ caused by the numerical integration process of noisy signals can be linearly approximated by

$$ v_{d,k} = \frac{v_{k_l+1} - v_{k_l}}{t_{k_l+1} - t_{k_l}}(t_k - t_{k_l}) + v_{k_l} \tag{12}$$

for each time window $t_{k_l} \leq t_k \leq t_{k_l+1}$. Then, the estimated induced-motion velocity is

$$ \hat{v}_k = v_k - v_{d,k} \tag{13}$$

Equations (10), (12) and (13) are similar to the algorithm known as Zero Velocity Updates (ZVU) as computed in [23], [42], [43]. Then, the Cartesian position ${}^{G}p_k$ is estimated by the numerical integration of $\hat{v}_k$. For example, with the Euler method, the IMU Cartesian position is computed at sample k by

$$ {}^{G}p_k = {}^{G}p_{k-1} + (t_k - t_{k-1})\, m_{d,k}\, {}^{G}\hat{v}_{k-1} \tag{14}$$

III. TESTBED AND EXPERIMENTAL RESULTS

A robot testbed was implemented, which includes the designed IMU device, a motion capture system *OptiTrack*™ as a ground truth, and a KUKA KR 16 industrial robot (shown in Figure 5) with its KRC4 controller. The *OptiTrack*™ system consists of 12 Prime 17W PoE (Power over Ethernet) cameras with a resolution of 1664×1088 pixels, an eSync2 data synchronizer and a NETGEAR ProSafe GS716T router. This router has the function of routing data packets from one network to another and of serving the *OptiTrack*™ system to communicate the central computer with the robot control unit. During human-robot interaction, the robot is signalled to start the operation to acquire the skill as in [33]. Afterwards, the spatial human motion task begins. The task consists of a human hand spatial motion to form a 3D trajectory using the IMU device. The main idea is to estimate its Cartesian trajectories and orientation and replicate it using the KUKA industrial robot.

The proposed design of the IMU device incorporates a motion processing unit (MPU), the MPU-6050 sensor, that combines a MEMS 3-axis accelerometer and a 3-axis gyroscope in a single chip. The MPU has a digital output resolution of 16 *bits* with a measurement resolution configured to $\pm 2°$ and $\pm 250°/s$. The sample frequency of the *Arduino*™ electronic platform and the *Bluetooth*® wireless communication is 260 Hz. The complete electronic device is shown in Figure 6 and the used device with its visual markers is shown in Figure 7.

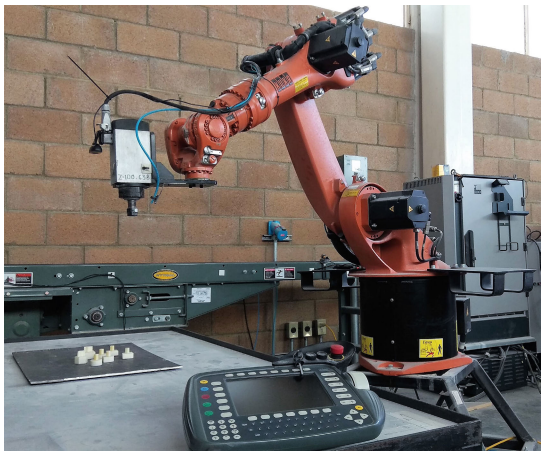

FIGURE 5. KUKA KR 16 industrial robot.

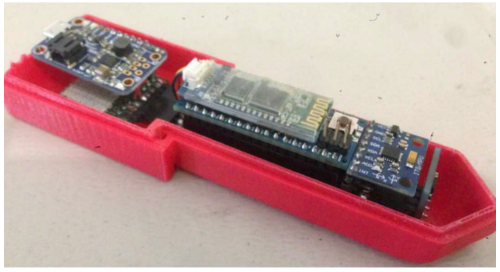

FIGURE 6. Device with the IMU.

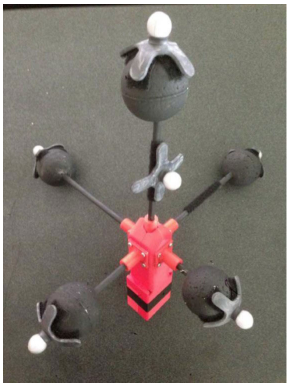

FIGURE 7. Visual markers for the motion capture system.

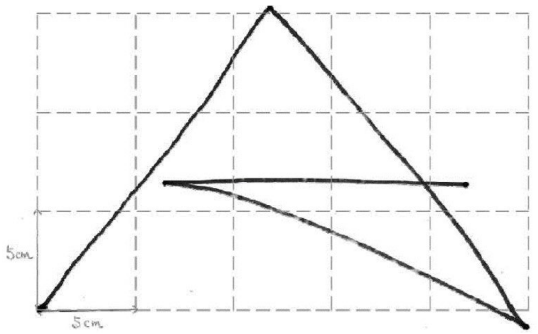

FIGURE 8. Proposed trajectory of letter "A".

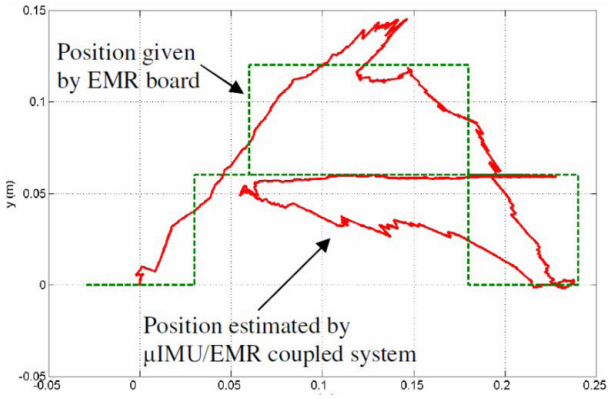

FIGURE 9. Results from handwriting estimation in [20].

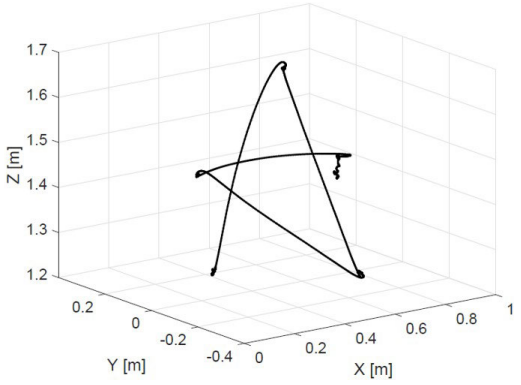

FIGURE 10. Actual trajectory made by hand.

A. VALIDATION

In this subsection, the orientation and estimation of a reference task was performed using the procedures from section II. This reference task consisted in drawing a letter "A" similar to the proposed methodology in [20] for handwriting estimation based on IMU and electromagnetic resonance motion detection (see Figure 8). The Tsang's position estimation results are shown in Figure 9.

In order to validate the proposed approach of IMU-based estimation, a three-dimensional version of the letter "A" (shown in Figure 10) was made by a human operator and recorded with the *OptiTrack*™ for comparison with the actual motion of the human operator. The motion capture of the human hand trajectories is illustrated in Figure 11. The goal was to replicate this trajectory using the KUKA KR 16 industrial robot programmed only with the trajectory estimated from the IMU data without using measurements from the motion capture system.

Using the procedures of section II, the orientation and position of the trajectory of Figure 10 were estimated from the IMU data. The threshold value U for Equation (10) was empirically chosen. The acceleration was transformed to the global reference frame f_G with a removed gravity vector and filtered by a low-pass Butterworth filter of order one.

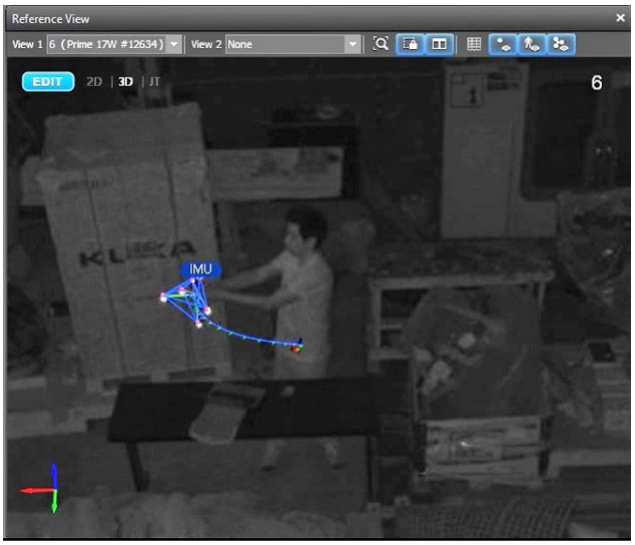

FIGURE 11. Motion capture system OptiTrack™.

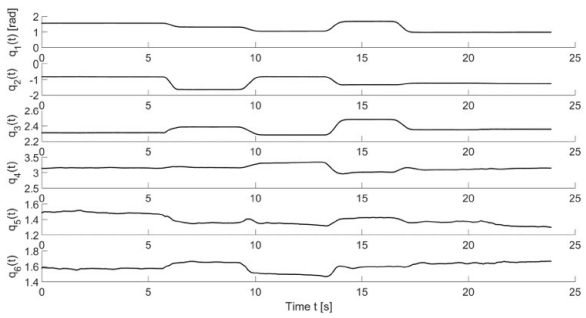

FIGURE 12. Position trajectories of the robot joints.

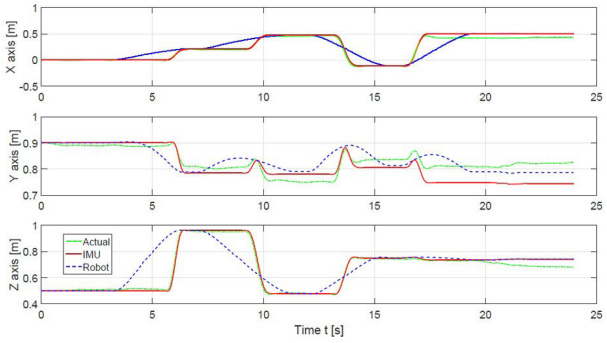

FIGURE 13. Time response of the Cartesian position trajectories.

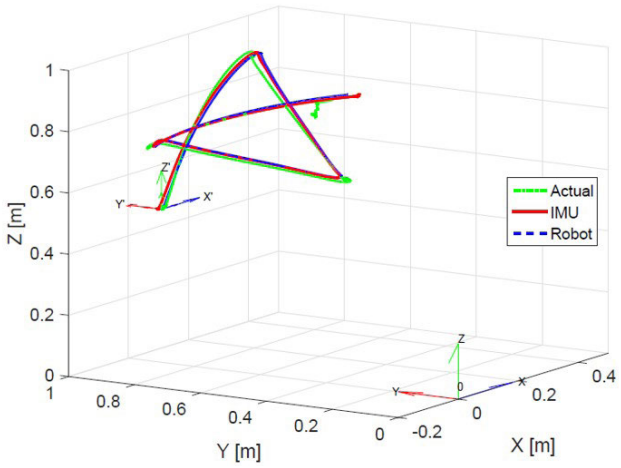

FIGURE 14. Experimental results for letter "A" in 3D space.

The Cartesian position trajectory of the human hand estimated from the IMU was scaled to the workspace of the KUKA KR 16 robot and the corresponding joint trajectories were computed. The kinematics for the KUKA robot were obtained by means of the Denavit-Hartenberg notation. So, the joint positions were programmed in the robot's controller and are shown in Figure 12. The Kuka Robot Language (KRL) was used to program the robot using point-to-point (PTP) instructions in joint coordinates.

In order to generate a continuous, human-like, smooth motion along the emulated path, point approximation was used in the robot controller (C_PTP motion). This behaviour can be observed in Figure 13 with the Cartesian trajectory performed by the robot versus time. As it is observed, the robot program generates trajectories made to avoid the abrupt changes in each of the 3 axis, generating a smooth motion along some points in the trajectory. For that reason, it seems that the robot's path deviates a lot from that IMU registered path as shown in Figure 13. However, it can also be observed that the robot's end-effector moves through the same points of the IMU registered trajectory but at a different time. This means that the path of the robot in Cartesian space is very close to the one estimated from the IMU data as seen in Figure 14.

In Figures 14 and 15, three data sets were plotted. The first data set was obtained from the actual operator's hand as registered by the *OptiTrack*™ system (Actual).

The following data set was the path estimated from the IMU data (IMU), and the last data set was obtained from the spatial motion as registered in the controller of the KUKA KR 16 robot (Robot). Figure 15 shows a projection in the XZ plane of Figure 14, where the difference in paths is clearer.

B. ERROR ANALYSIS

In order to quantify the performance of the proposed methodology and the experimental results, the estimation and tracking error was plotted. The estimation error vs time is the L2-norm difference between the actual human motion and the value registered by the IMU (Actual-IMU). The tracking error vs time is the L2-norm difference between the value registered by the IMU and the robot (IMU-Robot). In both cases, the mean and standard deviation were computed.

During experimental trials, it was noticed that the position error while moving along a trajectory was very much related to the motion detection given by equation (10). In this equation, the value of the variance $V_{k,M}$ was very important, specially when the trajectory contained abrupt changes (as it is the case in forming the letter "A"). During experiments,

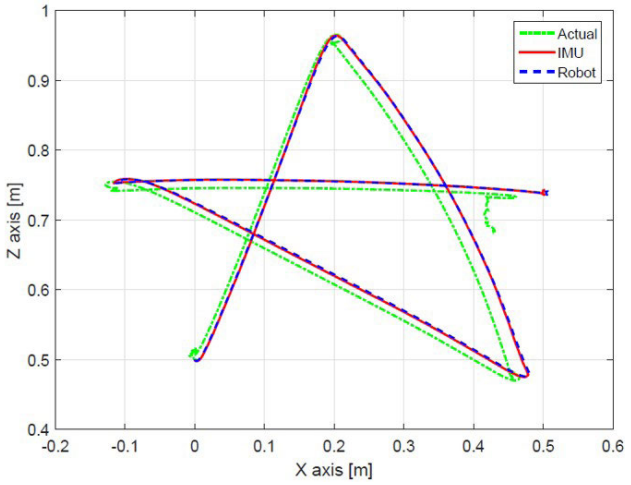

FIGURE 15. Projection of letter "A" in 2-dimensional space.

TABLE 2. Path estimation RMSE for different threshold values for the "A" path.

Threshold (U)	Acceleration (absolute)	Acceleration (L2-norm)	Acceleration (Variance)
0.01	2.4643	2.4642	0.0605
0.015	0.4079	0.6295	0.049
0.02	0.3829	1.2759	0.05
0.025	0.3293	0.3994	0.05
0.03	0.2163	0.3868	0.0519
0.04	0.1307	0.3189	0.0552
0.05	0.0964	0.1277	0.0578
0.06	0.078	0.1099	0.0593
0.07	0.0627	0.0724	0.0601
0.08	0.0953	0.0633	0.0618
0.09	0.0605	0.058	0.0648
0.1	0.0682	0.0574	0.0677

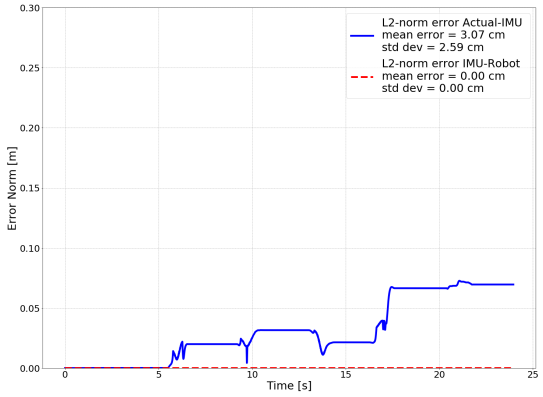

FIGURE 16. Error for the letter "A".

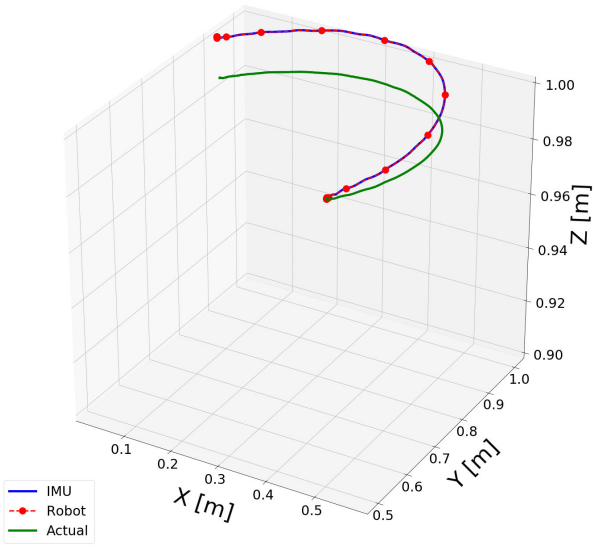

FIGURE 17. Experimental results for C-shape in 3D space.

the sensitivity was lower using the variance value than when using the absolute value of the acceleration or the L2-norm. Table 2 is an example of the results for the letter "A".

In the Table 2, there is a comparison of the numerical results of the RMSE (root-mean-square error) for the path estimation in 3D of the A-shape for different detection threshold values in the first column ranging from 0.01 to 0.1. The second column indicates the RMSE value obtained using the absolute magnitude of each acceleration component. The third column shows the RMSE using the L2-norm of the acceleration and the last column gives the RMSE using the variance value of the acceleration. As it can be seen, the RMSE is lower for the variance case than for the absolute acceleration or the L2-norm. In practice, the variance case was less sensitive within the threshold range.

This in terms of the spatial error vs time is shown in Figure 16. The error from the actual motion carried out by the operator estimated from the IMU (Actual-IMU), and the tracking error vs time (IMU-Robot) are shown. For these errors, the mean and standard deviation are computed.

Similar to section III-A, another smoother spatial path was tested by drawing a C-shape form in free-space. Figure 17 shows the recorded path as accomplished by the human operator; of which the error is shown in Figure 18. The mean and standard deviation of the L2-norm errors were also computed.

As it can be seen in all experiments, the tracking error is very small between the Cartesian path estimated from the IMU data and the one performed by the robot. The most notable error or shift is between the path estimated from IMU data and the actual human movement, that is, the estimation error (for example, after 17 seconds in Figure 16). As it can be seen in Figure 16, the mean of the estimation error for the path of "A" is at around 3 cm, while the mean of estimation error is less than 1 cm in the C-shape (Figure 18).

The position estimate worsens as time passes, mainly due to the drift effect of numerical integration (integration explained in section II), the estimate's worsening seems to be affected by abrupt movements (as in the case of the path of "A") and by the location of the visual markers. The error estimation is smaller as the motion of the path is smoother

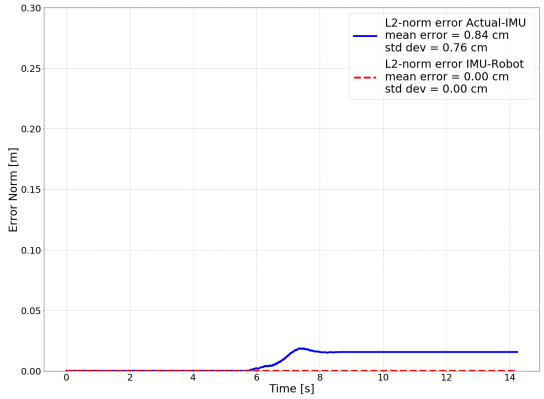

FIGURE 18. Error for the C-shape.

like in the C-shape. In related works, the estimation errors from the IMU usually have magnitudes of several centimeters (for position) or sexagesimal degrees (for orientation) as seen in [20], [35], [44], [45]. Although there are filtering stages, this estimation error is also due to the noise level of the measurements of the acceleration and speed.

In our experimental results, it can be mentioned that the trajectories are reconstructed in their shape and with a certain degree of precision (although still limited) from the IMU data. The current quality of trajectory estimation could not be sufficient while working in constraint motion; however, it is acceptable for free-motion applications such as painting, spraying or when the error tolerance allows the operation such as in the case of gluing or welding.

IV. CONCLUSION AND FUTURE WORK

Robot skill acquisition using LfD techniques involves a high-level stage in charge of learning connected actions, whereas a low-level stage is concerned with motor coordination to reproduce and imitate an observed human path. This paper is concerned with the acquisition of a path-following motion at the low-level stage to facilitate robot task-level programming using the LfD technique. For the low-level stages of motion acquisition, the IMU-based methodology is proposed to be used as input to acquire an object motion path in Cartesian space as a low-cost, portable, simple-to-implement alternative to other sensing systems for outdoor and indoor applications, requiring only accelerometers and gyroscopes.

During tests, the human operator moved the IMU device in free-space; then, the Cartesian position and orientation were computed with the methodology proposed in this work. With this estimated information and the inverse kinematics of the robot, the continuous-time functions of the joint variables were obtained in order to be programmed into the robot controller.

As it is well known, the CVS have very small magnitudes of error when capturing motion paths in constrained indoor environments. The proposed approach for trajectory estimation from IMU does not intend to replace CVS but rather uses CVS as a precise, reliable and repeatable experimental platform to quantify the estimation quality of the presented IMU-based algorithms for comparison with the actual motion of the human operator.

The proposed methodology is robust having various advantages over other algorithms and sensing systems as follows:

- Motion detection under uncertainties due to gravity acceleration, calibration, and small vibrations from the so-called artifacts (such as breathing).
- Flexibility outdoors. Since it is portable and not restricted to structured environments requiring external equipment for detection.
- Robust to light varying conditions, occlusions, background acoustic noise or wind (when used outdoors).

In addition:

- It is not limited to the rigidity of the wearable equipment (such as in exo-skeletons) and can detect events such as jumping or turning.
- During motion with "constant" speed, the acceleration is around zero.
- The resultant path at the low-level of the LfD technique considers small errors that could be considered acceptable for some robot tasks in free-space (e.g. painting).
- The methodology can be adapted/modified for heterogeneous robots considering only its different programming languages.
- Cost-effective specifically compared to CVS.

Further work has been envisaged to test the overall performance in constrained motion. One of the challenges is to reduce the estimation error taking advantage of this platform and methodology to quantify and compare it. Some approaches to reduce the magnitude of the error could consist of modifying the algorithm in the stages of filtering, numerical integration or in the detection of movement as well as complement the scheme with other devices and sensor fusion techniques. For example, arrangements with several IMU, magnetometers, RF ID devices, GPS, adding points or marks for error correction, and so on.

APPENDIX A
AKF PSEUDOCODE

As explained in [40], the start of "*a priori*" system estimation consist in the following:

1) The angular velocities ω_x, ω_y and ω_z measured by the gyro sensor are used to fill the matrix

$$\Omega^n_{nb} = \begin{bmatrix} 0 & -\omega_x & -\omega_y & -\omega_z \\ \omega_x & 0 & \omega_z & -\omega_y \\ \omega_y & -\omega_z & 0 & \omega_x \\ \omega_z & \omega_y & -\omega_x & 0 \end{bmatrix};$$

2) calculation of the discrete-time state transition matrix $A_k = I + \frac{1}{2}\Omega^n_{nb}T$, where I is the identity matrix of appropriate dimensions and T is the time step between each execution of the algorithm in the digital system;
3) calculation of the "*a priori*" system state estimation $\hat{q}_k^- = A_k\hat{q}_{k-1}$, where $\hat{q}_{k-1}$ is the "*a posteriori*" system state estimation at the previous step;

4) calculation of the "*a priori*" noise covariance matrix $P_k^- = A_k P_{k-1} A_k^{\mathrm{T}} + Q_{k-1}$, where P_{k-1} is the "a posteriori" error covariance matrix at the previous filter iteration and Q_{k-1} is the process noise covariance matrix.

Start of the correction stage 1:

1) calculation of the Jacobian matrix

$$H_{k1} = \begin{bmatrix} -2q_2 & 2q_3 & -2q_0 & 2q_1 \\ 2q_1 & 2q_0 & 2q_3 & 2q_2 \\ 2q_0 & -2q_1 & -2q_2 & 2q_3 \end{bmatrix},$$

from the quaternion components $q_0,\ q_1,\ q_2,\ q_3$;
2) calculation of the Kalman gain $K_{k1} = P_k^- H_{k1}^{\mathrm{T}} (H_{k1} P_k^- H_{k1}^{\mathrm{T}} + V_{k1} R_{k1} V_{k1}^{\mathrm{T}})^{-1}$, where R_{k1} is the measurement noise covariance matrix, directly depending on the noise of the accelerometer, plus other error sources that are considered as noise. V_{k1} is a Jacobian matrix of the partial derivatives with respect to the quaternion and to the noise, such that V_{k1} is an identity matrix if the noise of the accelerometer is considered noncorrelated with the current angular position;
3) reading of the accelerometer data $z_{k1} = [a_x\ a_y\ a_z]^T$;
4) estimation of gravity vector as

$$h_1(\hat{q}_k^-) = \begin{bmatrix} 2q_1q_3 - 2q_0q_2 \\ 2q_0q_1 + 2q_2q_3 \\ q_0^2 - q_1^2 - q_2^2 + q_3^2 \end{bmatrix};$$

5) calculation of the correction factor
$q_{\epsilon 1} = K_{k1}(z_{k1} - h_1(\hat{q}_k^-))$
$= q_{\epsilon 1,0} + q_{\epsilon 1,1} + q_{\epsilon 1,2} + 0 \cdot q_{\epsilon 1,3}$
with $q_{\epsilon 1,3}$ equal to zero;
6) calculation of the "*a posteriori*" state estimation $\hat{q}_{k1} = \hat{q}_k^- + q_{\epsilon 1}$;
7) calculation of the "*a posteriori*" error covariance matrix $P_{k1} = (I - K_{k1} H_{k1}) P_k^-$.

Start of the correction stage 2:

1) calculation of the Jacobian matrix

$$H_{k2} = \begin{bmatrix} 2q_3 & 2q_2 & 2q_1 & 2q_0 \\ 2q_0 & -2q_1 & -2q_2 & -2q_3 \\ -2q_1 & -2q_0 & 2q_3 & 2q_2 \end{bmatrix};$$

from the quaternion components $q_0,\ q_1,\ q_2,\ q_3$;
2) calculation of the Kalman gain $K_{k2} = P_k^- H_{k2}^{\mathrm{T}} (H_{k2} P_k^- H_{k2}^{\mathrm{T}} + V_{k2} R_{k2} V_{k2}^{\mathrm{T}})^{-1}$, where R_{k2} is the measurement noise covariance matrix, directly depending on the noise of the magnetic sensor, plus other error sources that are considered as noise, also V_{k2} is an identity matrix if the noise of the magnetic compass is considered noncorrelated with the current angular position;
3) reading of the magnetic compass data $z_{k2} = [m_x\ m_y\ m_z]^T$;

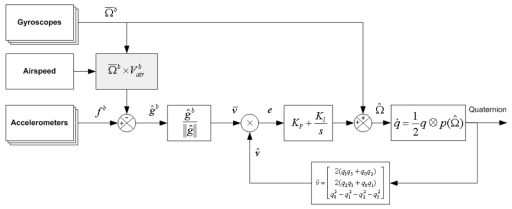

FIGURE 19. Scheme of the ECF. Taken from [35].

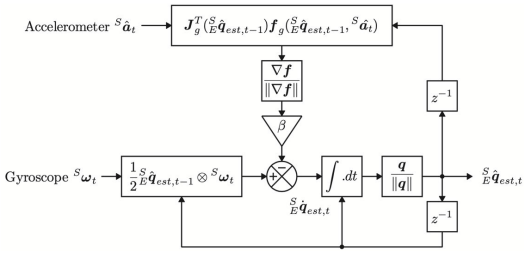

FIGURE 20. Scheme of the DGA. Taken from [38].

4) estimation of the magnetic field as

$$h_2(\hat{q}_k^-) = \begin{bmatrix} 2q_1q_2 + 2q_0q_3 \\ q_0^2 - q_1^2 - q_2^2 - q_3^2 \\ 2q_2q_3 - 2q_0q_1 \end{bmatrix};$$

5) calculation of the correction factor
$q_{\epsilon 2} = K_{k2}(z_{k2} - h_2(\hat{q}_k^-))$
$= q_{\epsilon 2,0} + 0 \cdot q_{\epsilon 2,1} + 0 \cdot q_{\epsilon 2,2} + q_{\epsilon 2,3}$
with $q_{\epsilon 2,1}$ and $q_{\epsilon 2,2}$ equal to zero;
6) calculation of the "*a posteriori*" state estimation $\hat{q}_k = \hat{q}_{k1} + q_{\epsilon 2}$;
7) calculation of the "*a posteriori*" error covariance matrix $P_k = (I - K_{k2} H_{k2}) P_{k1}$.

APPENDIX B
IMPLEMENTED FILTER PARAMETERS

The following filters and parameters were implemented for the research in this paper.

A. COMPLEMENTARY FILTER (CF)

$$\theta_k = [\alpha\ (\theta_{k-1} + \omega_k \cdot dt)] + (1 - \alpha)\theta_a \tag{15}$$

Parameters:

- $\alpha = 0.995$

B. EXPLICIT COMPLEMENTARY FILTER (ECF)

Parameters:

- $K_P = 0.5$
- $K_I = 0.1$

C. DESCENDENT GRADIENT ALGORITHM (DGA)

Parameters:

- $beta = 0.0756$

D. ADAPTIVE KALMAN FILTER (AKF)

Parameters:

- Matrix for initial covariance: $P_k = (0.122\, I_4) + 0.003$

E. QUATERNION-BASED ADAPTIVE FILTER (QBAF)

Parameters:

- α gain is adaptive
- $\bar{\alpha} = 0.006$ (This was the gain for best results in static conditions)

REFERENCES

[1] M. Kyrarini, M. A. Haseeb, D. Ristić-Durrant, and A. Gräser, "Robot learning of industrial assembly task via human demonstrations," *Auto. Robots*, vol. 43, no. 1, pp. 239–257, Jan. 2019, doi: 10.1007/s10514-018-9725-6.

[2] M. Menolotto, D.-S. Komaris, S. Tedesco, B. O'Flynn, and M. Walsh, "Motion capture technology in industrial applications: A systematic review," *Sensors*, vol. 20, no. 19, p. 5687, Oct. 2020.

[3] M. Field, Z. Pan, D. Stirling, and F. Naghdy, "Human motion capture sensors and analysis in robotics," *Ind. Robot, Int. J.*, vol. 38, no. 2, pp. 163–171, Mar. 2011.

[4] X. Wang, D. Liu, Y. Tao, and Y. Cui, "An optimized path planning method for off-line programming of a industrial robot," in *Proc. Int. Conf. Comput. Sci. Electron. Eng. (ICCSEE)*, vol. 3, Mar. 2012, pp. 57–60.

[5] Z. Yin, X. Yuan, G. Zhang, and L. Wu, "Automated generation of robot MAG surfacing path for remanufacturing system," in *Proc. IEEE Int. Conf. Mechatronics Autom.*, Aug. 2012, pp. 1347–1351.

[6] M. Dinham and G. Fang, "Weld seam detection using computer vision for robotic arc welding," in *Proc. IEEE Int. Conf. Autom. Sci. Eng. (CASE)*, Aug. 2012, pp. 771–776.

[7] J. Hatwig, P. Minnerup, M. F. Zaeh, and G. Reinhart, "An automated path planning system for a robot with a laser scanner for remote laser cutting and welding," in *Proc. IEEE Int. Conf. Mechatronics Autom.*, Aug. 2012, pp. 1323–1328.

[8] P. Tsarouchi, S. Makris, and G. Chryssolouris, "Human–robot interaction review and challenges on task planning and programming," *Int. J. Comput. Integr. Manuf.*, vol. 29, no. 8, pp. 916–931, Aug. 2016.

[9] C. R. G. Dreher, M. Wächter, and T. Asfour, "Learning object-action relations from bimanual human demonstration using graph networks," *IEEE Robot. Autom. Lett.*, vol. 5, no. 1, pp. 187–194, Jan. 2020.

[10] Y. Zhou, J. Gao, and T. Asfour, "Movement primitive learning and generalization: Using mixture density networks," *IEEE Robot. Autom. Mag.*, vol. 27, no. 2, pp. 22–32, Jun. 2020.

[11] S. Calinon, F. Guenter, and A. Billard, "On learning, representing, and generalizing a task in a humanoid robot," *IEEE Trans. Syst., Man Cybern. B, Cybern.*, vol. 37, no. 2, pp. 286–298, Apr. 2007.

[12] M. Sanzari, V. Ntouskos, and F. Pirri, "Discovery and recognition of motion primitives in human activities," *PLoS ONE*, vol. 14, no. 4, pp. 1–39, Apr. 2019, doi: 10.1371/journal.pone.0214499.

[13] N. Figueroa, S. Faraji, M. Koptev, and A. Billard, "A dynamical system approach for adaptive grasping, navigation and co-manipulation with humanoid robots," in *Proc. IEEE Int. Conf. Robot. Autom. (ICRA)*, May 2020, pp. 7676–7682.

[14] W. Amanhoud, M. Khoramshahi, M. Bonnesoeur, and A. Billard, "Force adaptation in contact tasks with dynamical systems," in *Proc. IEEE Int. Conf. Robot. Autom. (ICRA)*, May 2020, pp. 6841–6847.

[15] T. Asfour, F. Paus, M. Waechter, L. Kaul, S. Rader, P. Weiner, S. Ottenhaus, R. Grimm, Y. Zhou, and M. Grotz, "ARMAR-6: A high-performance humanoid for human-robot collaboration in real-world scenarios," *IEEE Robot. Autom. Mag.*, vol. 26, no. 4, pp. 108–121, Dec. 2019.

[16] D. Tome, P. Peluse, L. Agapito, and H. Badino, "XR-EgoPose: Egocentric 3D human pose from an HMD camera," in *Proc. IEEE/CVF Int. Conf. Comput. Vis. (ICCV)*, Oct. 2019, pp. 7728–7738.

[17] P. Tsarouchi, A. Athanasatos, S. Makris, X. Chatzigeorgiou, and G. Chryssolouris, "High level robot programming using body and hand gestures," *Procedia CIRP*, vol. 55, pp. 1–5, Jan. 2016. [Online]. Available: https://www.sciencedirect.com/science/article/pii/S2212827116309544

[18] L. Mauro, F. Puja, S. Grazioso, V. Ntouskos, M. Sanzari, E. Alati, and F. Pirri, "Visual search and recognition for robot task execution and monitoring," *CoRR*, vol. abs/1902.02870, pp. 1–16, Feb. 2019. [Online]. Available: http://arxiv.org/abs/1902.02870

[19] X. Yun, J. Calusdian, E. R. Bachmann, and R. B. McGhee, "Estimation of human foot motion during normal walking using inertial and magnetic sensor measurements," *IEEE Trans. Instrum. Meas.*, vol. 61, no. 7, pp. 2059–2072, Jul. 2012.

[20] C. C. Tsang, P. H. W. Leong, G. Zhang, C. F. Chung, Z. Dong, G. Shi, and W. J. Li, "Handwriting tracking based on coupled μIMU/electromagnetic resonance motion detection," in *Proc. IEEE Int. Conf. Robot. Biomimetics (ROBIO)*, Dec. 2007, pp. 377–381.

[21] A. Cavallo, A. Cirillo, P. Cirillo, G. De Maria, P. Falco, C. Natale, and S. Pirozzi, "Experimental comparison of sensor fusion algorithms for attitude estimation," *IFAC Proc. Volumes*, vol. 47, no. 3, pp. 7585–7591, 2014.

[22] B. Wagstaff, V. Peretroukhin, and J. Kelly, "Robust data-driven zero-velocity detection for foot-mounted inertial navigation," *IEEE Sensors J.*, vol. 20, no. 2, pp. 957–967, Jan. 2020.

[23] J. Wu, Z. Zhou, H. Fourati, R. Li, and M. Liu, "Generalized linear quaternion complementary filter for attitude estimation from multisensor observations: An optimization approach," *IEEE Trans. Autom. Sci. Eng.*, vol. 16, no. 3, pp. 1330–1343, Jul. 2019.

[24] A. Filippeschi, N. Schmitz, M. Miezal, G. Bleser, E. Ruffaldi, and D. Stricker, "Survey of motion tracking methods based on inertial sensors: A focus on upper limb human motion," *Sensors*, vol. 17, no. 6, p. 1257, Jun. 2017. [Online]. Available: https://www.mdpi.com/1424-8220/17/6/1257

[25] M. A. Wirth, G. Fischer, J. Verdú, L. Reissner, S. Balocco, and M. Calcagni, "Comparison of a new inertial sensor based system with an optoelectronic motion capture system for motion analysis of healthy human wrist joints," *Sensors*, vol. 19, no. 23, p. 5297, Dec. 2019. [Online]. Available: https://www.mdpi.com/1424-8220/19/23/5297

[26] F. Kluge, H. Gaßner, J. Hannink, C. Pasluosta, J. Klucken, and B. Eskofier, "Towards mobile gait analysis: Concurrent validity and test-retest reliability of an inertial measurement system for the assessment of spatio-temporal gait parameters," *Sensors*, vol. 17, no. 7, p. 1522, Jun. 2017. [Online]. Available: https://www.mdpi.com/1424-8220/17/7/1522

[27] Y.-S. Cho, S.-H. Jang, J.-S. Cho, M.-J. Kim, H. D. Lee, S. Y. Lee, and S.-B. Moon, "Evaluation of validity and reliability of inertial measurement unit-based gait analysis systems," *Ann. Rehabil. Med.*, vol. 42, no. 6, pp. 872–883, Dec. 2018. [Online]. Available: http://www.e-arm.org/journal/view.php?number=4055

[28] M. Al-Amri, K. Nicholas, K. Button, V. Sparkes, L. Sheeran, and J. Davies, "Inertial measurement units for clinical movement analysis: Reliability and concurrent validity," *Sensors*, vol. 18, no. 3, p. 719, Feb. 2018.

[29] A. Amorim, D. Guimares, T. Mendona, P. Neto, P. Costa, and A. P. Moreira, "Robust human position estimation in cooperative robotic cells," *Robot. Comput.-Integr. Manuf.*, vol. 67, Feb. 2021, Art. no. 102035. [Online]. Available: http://www.sciencedirect.com/science/article/pii/S0736584520302465

[30] D. Xu and Q. Wang, "On-board training strategy for IMU-based real-time locomotion recognition of transtibial amputees with robotic prostheses," *Frontiers Neurorobot.*, vol. 14, p. 47, Oct. 2020. [Online]. Available: https://www.frontiersin.org/article/10.3389/fnbot.2020.00047

[31] G. Du, Y. Liang, C. Li, P. X. Liu, and D. Li, "Online robot kinematic calibration using hybrid filter with multiple sensors," *IEEE Trans. Instrum. Meas.*, vol. 69, no. 9, pp. 7092–7107, Sep. 2020.

[32] R. W. S. M. de Oliveira, R. Bauchspiess, L. H. S. Porto, C. G. de Brito, L. F. C. Figueredo, G. A. Borges, and G. N. Ramos, "A robot architecture for outdoor competitions," *J. Intell. Robot. Syst.*, vol. 99, nos. 3–4, pp. 629–646, Sep. 2020, doi: 10.1007/s10846-019-01140-9.

[33] I. Lopez-Juarez, R. Rios-Cabrera, E. Rojas-Sanchez, A. Maldonado-Ramirez, and G. Lefranc, "Grounding the lexicon for human-robot interaction during the manipulation of irregular objects," in *Proc. 7th Int. Conf. Comput. Commun. Control (ICCCC)*, May 2018, pp. 282–288.

[34] D. Serrano, F. Ayazi, O. Brand, I. Dufour, S. Heinrich, and F. Josse, Eds., *Resonant MEMS: Fundamentals, Implementation, and Application*, 1st ed. Weinheim, Germany: Wiley-VCH Verlag, 2015.

[35] M. Euston, P. Coote, R. Mahony, J. Kim, and T. Hamel, "A complementary filter for attitude estimation of a fixed-wing UAV," in *Proc. IEEE/RSJ Int. Conf. Intell. Robots Syst.*, Sep. 2008, pp. 340–345.

[36] D. D. Quoc, J. Sun, V. N. Le, and N. N. Tan, "Sensor fusion based on complementary algorithms using MEMS IMU," *Int. J. Signal Process., Image Process. Pattern Recognit.*, vol. 8, no. 2, pp. 313–324, Feb. 2015.
[37] R. Valenti, I. Dryanovski, and J. Xiao, "Keeping a good attitude: A quaternion-based orientation filter for IMUs and MARGs," *Sensors*, vol. 15, no. 8, pp. 19302–19330, Aug. 2015.
[38] S. O. H. Madgwick, A. J. L. Harrison, and R. Vaidyanathan, "Estimation of IMU and MARG orientation using a gradient descent algorithm," in *Proc. IEEE Int. Conf. Rehabil. Robot.*, Jun. 2011, pp. 1–7.
[39] R. Kumar, M. Bhargavapuri, A. M. Deshpande, S. Sridhar, K. Cohen, and M. Kumar, "Quaternion feedback based autonomous control of a quadcopter UAV with thrust vectoring rotors," in *Proc. Amer. Control Conf. (ACC)*, Jul. 2020, pp. 3828–3833.
[40] S. Sabatelli, M. Galgani, L. Fanucci, and A. Rocchi, "A double-stage Kalman filter for orientation tracking with an integrated processor in 9-D IMU," *IEEE Trans. Instrum. Meas.*, vol. 62, no. 3, pp. 590–598, Mar. 2013.
[41] A. Makni, H. Fourati, and A. Y. Kibangou, "Adaptive Kalman filter for MEMS-IMU based attitude estimation under external acceleration and parsimonious use of gyroscopes," in *Proc. Eur. Control Conf. (ECC)*, Jun. 2014, pp. 1379–1384.
[42] I. Skog, P. Handel, J. O. Nilsson, and J. Rantakokko, "Zero-velocity detection—An algorithm evaluation," *IEEE Trans. Biomed. Eng.*, vol. 57, no. 11, pp. 2657–2666, Nov. 2010.
[43] K. Abdulrahim, T. Moore, C. Hide, and C. Hill, "Understanding the performance of zero velocity updates in MEMS-based pedestrian navigation," *Int. J. Adv. Technol.*, vol. 5, no. 1, pp. 53–60, 2014.
[44] C. B. Abellanosa, R. P. J. Lugpatan, and D. A. D. Pascua, "Position estimation using inertial measurement unit (IMU) on a quadcopter in an enclosed environment," *Int. J. Comput., Commun. Instrum. Eng.*, vol. 3, no. 2, pp. 332–336, 2016.
[45] R. Pellois, L. Joris, and O. Bruls, "Robot control based on human motion analysis with IMU measurements," in *Proc. Robotix Acad. Conf. Ind. Robot.*, Jun. 2017, pp. 1–5.

ANGEL RODRIGUEZ-LIÑAN received the B.Eng. degree in electronics and the M.Sc. and Ph.D. degrees in electrical engineering from the Universidad Autónoma de Nuevo León, Mexico, in 2003, 2005, and 2009, respectively. He is a full-time Professor with the Graduate School of Electrical Engineering, Universidad Autónoma de Nuevo León, where he is a member of the Mechatronics Research Group. His areas of interests include analysis, estimation, control and instrumentation in dynamical systems, robotics, and biomechatronics.

ISMAEL LOPEZ-JUAREZ received the B.Eng. degree from the National Autonomous University of Mexico, the M.Sc. degree from UMIST, in 1996, and the Ph.D. degree in intelligent robotics from Nottingham Trent University, U.K., in 2000. He is currently the Leader of the Intelligent Manufacturing Laboratory, CINVESTAV. He has published over 200 articles, has supervised eight Ph.D., 17 M.Sc., and seven B.Eng. students. He has one patent and has been responsible for several technological projects and technology transfer within the industry. His areas of interests include instrumentation, self-adaptive industrial robots, neural networks, and machine vision. He is a member of the National Researchers Systems in Mexico (SNI), Level II. He is a member of the Editorial Committee for the IEEE Latin America Transactions. He has acted as a regular reviewer for major journals in his field. He is a Guest Editor for the *Transactions on Intelligent Welding Manufacturing* (Springer).

ALAN MALDONADO-RAMIREZ received the B.Eng. degree in electronics from the Instituto Tecnologico de Tampico, Mexico, in 2014, and the M.Sc. degree robotics and advanced manufacturing from CINVESTAV, in 2018, where he is currently pursuing the Ph.D. degree. His current research interests include artificial neural networks applied to robotics and manufacturing, electronics design, and mobile robotics.

ANTONIO ZALAPA-ELIAS received the B.Eng. degree in mechatronics and the M.S. degree in electrical engineering from the Universidad Autónoma de Nuevo León, Mexico. His thesis focused on the analysis and processing of signals from IMUs to estimation of orientation and position as well as on the modelling and programming of industrial robots.

LUIS TORRES-TREVIÑO received the B.Eng. degree in electronics, the M.Sc. degree in electrical engineering, and the Ph.D. degree in artificial intelligence. He has been a consultant for more than 25 years developing diverse solutions using intelligent systems for productive processes of diverse industries. He is currently a Researcher and a Professor with the Universidad Autonoma de Nuevo Leon, Mexico. He is the author of more than 150 publications. His research interests include the IoT, AI, autonomous learning, development of devices for medical diagnosis, and platforms for swarm robotics. He is a member of the Mexican Society of Artificial Intelligence (SMIA) and the National System of Researchers (SNI) Level 1.

JOSE LUIS NAVARRO-GONZALEZ received the degree in mechatronics engineering from the Instituto Tecnológico de Saltillo and the master's and Ph.D. degrees in robotics and advanced manufacturing from the Centro de Investigación y de Estudios Avanzados del IPN. He is currently a General Manager at IJ Robotics, a company dedicated to research, development, and innovation in various schemes of mobile and industrial robots. His areas of expertise range from design of robotic systems to areas related to vision systems, CAD/CAM software technologies, and development of industrial robots' cells.

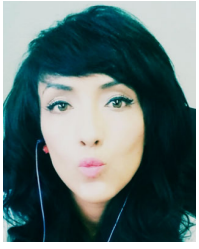

PAMELA CHIÑAS-SANCHEZ received the degree in mechatronics engineering from the Universidad Politécnica de Zacatecas, Zacatecas, México, in 2008, and the M.Sc. and Ph.D. degrees in robotics and advanced manufacturing from the Centro de Investigación y de Estudios Avanzados del IPN, Saltillo, México, in 2011 and 2015, respectively. She is currently a full-time Researcher with the Instituto Tecnologico de Saltillo (ITS). Her current research interests include artificial neural networks applied to robotics and manufacturing, quality control, and systems control.